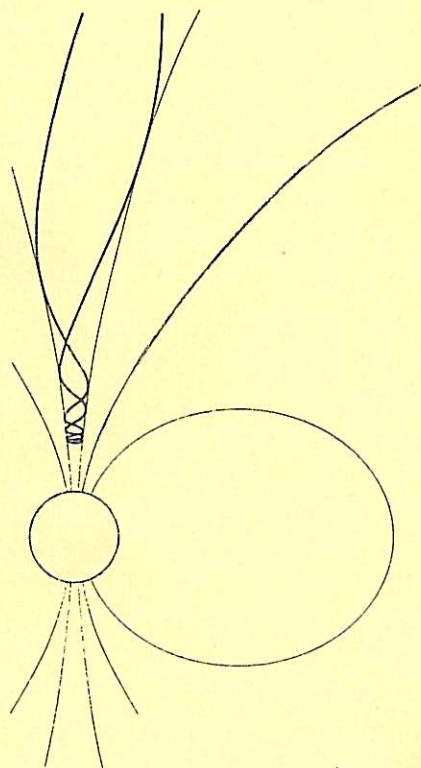


# Magnetospheric oscillations due to solar wind perturbations

Torbjörn Sundberg



*Master of Science Thesis  
Stockholm, Sweden 2005*



KTH Alfvén Laboratory



# Magnetospheric oscillations due to solar wind perturbations

Torbjörn Sundberg

February 2005

#### **Abstract**

A study of the magnetospheric reaction to sudden increases in the solar wind momentum flux has been conducted. Solar wind data from the ACE satellite have been compared to terrestrial magnetic field measurements and a particular interest has been paid to the pulsation magnetometer data from SANA. For those solar wind events that show a correlation to terrestrial magnetic storms, a leap in the absolute field can be seen as well as magnetospheric pulsations. Unfortunately, due to impulse saturation, a complete analysis of the nature of the pulsations is impossible.

### Sammanfattning

En studie av magnetosfäriska förändringar orsakade av plötsliga ökningar av solvindens dynamiska tryck har genomförts. Solvindsdata från ACE-satelliten har jämförts med magnetfältsmätningar från jordytan, med fokus på pulsationsmagnetometerdata från SANA. För de observerade solvindshändelser som hänger samman med jordmagnetiska stormar kan ett steg i det absoluta magnetfältet observeras såväl som magnetosfäriska pulsationer. Tyvärr kan ingen komplett analys av pulsationerna genomföras, då mätsignalen ofta är mättad.

# Contents

<b>1 Plasma Characteristics</b>	<b>3</b>
1.1 The Debye length . . . . .	3
1.2 Magneto-hydrodynamics . . . . .	4
1.3 Magneto-hydrodynamic waves . . . . .	4
1.4 Frozen-in field lines. . . . .	5
1.5 Collisionless shocks . . . . .	5
<b>2 Cosmic Plasmas</b>	<b>7</b>
2.1 The solar wind . . . . .	7
2.2 The Ionosphere . . . . .	7
2.3 The Magnetosphere . . . . .	8
2.3.1 Van Allen radiation belts . . . . .	8
<b>3 Data acquisition</b>	<b>9</b>
3.1 The ACE and Wind satellites . . . . .	9
3.2 SANAe pulsation magnetometer . . . . .	9
3.3 Absolute magnetometers . . . . .	10
3.3.1 The Dst-index . . . . .	10
<b>4 Magnetosphere and solar wind interaction</b>	<b>11</b>
4.1 The magnetopause . . . . .	11
4.1.1 The magnetopause current . . . . .	11
4.2 Magnetic storms . . . . .	12
<b>5 Methods of Analysis</b>	<b>13</b>
5.1 Shock speed . . . . .	13
5.1.1 Method of mass flux conservation . . . . .	14
5.1.2 WIND Measurements . . . . .	14
<b>6 Analysing the data</b>	<b>15</b>
6.1 Studied time period and data sources: . . . . .	15
6.1.1 Corrupt data samples . . . . .	15
6.2 Solar wind events . . . . .	15
6.3 Magnetometer data . . . . .	16
6.4 Propagation time calculations . . . . .	17
6.5 Solar wind speed calculations using WIND . . . . .	17
<b>7 Comments</b>	<b>32</b>
7.1 Magnetospheric propagation . . . . .	32
7.2 Event of 8 April . . . . .	32
7.3 Events of 24-25 October . . . . .	33
7.4 Event of 31 October . . . . .	33
7.5 Event of 22 January . . . . .	33
7.6 Conclusions . . . . .	34

## Chapter 1

# Plasma Characteristics

A plasma can be considered as a partially or fully ionised gas with a quasi neutral charge distribution, i.e., the numbers of negative and positive charges are macroscopically equal. It is often referred to as the fourth state of matter as plasmas show some very special characteristics, though it is not true in a strict thermodynamic point of view as the transition process from gas to plasma is a gradual one, there is no clean border between the two of them.

Some of the special qualities of a plasma will be described in the sections below.

### 1.1 The Debye length

One of the most important characteristics of a plasma is the Debye-length. Due to the mobility of the ions and electrons and the criterion of quasi-neutrality it is possible to express a relation between the maximum potential energy a charged particle can have and the kinetic energy.

Consider a one dimensional area with solely positive ions (no electrons), ranging from  $x = 0$  to  $x = d$ . This will yield the following potential energy difference  $\Delta W$  between the two borders for an electron:

$$\Delta W = e\Delta V = \frac{e^2 n_i d^2}{2\epsilon_0} \quad (1.1)$$

where  $e$  is the electron charge and  $n_i$  the ion density. This force cannot greatly exceed that of the kinetic energy of one dimension (as it thus would increase the thermal energy of the plasma), which in turn gives us a figure of the largest charge displacement allowed in the plasma, namely the Debye length,  $\lambda_d$ :

$$\frac{e^2 n_i \lambda_d^2}{2\epsilon_0} = kT_e/2 \quad (1.2)$$

$$\lambda_d = \sqrt{\frac{\epsilon_0 k T_e}{e^2 n_i}} \quad (1.3)$$

where  $T_e$  is the electron temperature and  $k$  the Boltzmann constant. The figure of the Debye length gives a good indication of the plasma shielding effect. This means that a larger charge in a plasma environment will attract particles of

opposite charge which in turn will serve to shield off its electric field at larger distances. It is often a useful approximation to assume that a particle will affect the environment up to the Debye length, after which it will be shielded and no longer be of any contribution.

## 1.2 Magneto-hydrodynamics

Due to the huge amount of particles involved, it is hard to treat and model a plasma based on individual particles, their motions and interaction. To overcome this problem, one often chooses to approach problems with a magneto-hydrodynamic model where one regards the plasma as a continuous conducting fluid. With the help of basic electric and magnetic theory, this fluid can then easily be described by the Maxwell equations ([2]),

$$\nabla \times \mathbf{E} = -\frac{\partial \mathbf{B}}{\partial t} \quad (1.4)$$

$$\nabla \times \mathbf{H} = \mathbf{i} + \frac{\partial \mathbf{D}}{\partial t} \quad (1.5)$$

$$\nabla \cdot \mathbf{D} = \xi \quad (1.6)$$

$$\nabla \cdot \mathbf{B} = 0 \quad (1.7)$$

Ohm's law and the equation of motion:

$$\mathbf{i} = \sigma(\mathbf{E} + \mathbf{v} \times \mathbf{B}) \quad (1.8)$$

$$\rho \frac{d\mathbf{v}}{dt} = \mathbf{i} \times \mathbf{B} - \nabla p \quad (1.9)$$

where  $\mathbf{E}$  is the electric field,  $\mathbf{D}$  the electric displacement,  $\mathbf{B}$  the magnetic flux density,  $\mathbf{H}$  the magnetic field strength,  $\mathbf{i}$  the current density,  $\rho$  the mass density,  $\xi$  the net charge density,  $\sigma$  the conductivity,  $\mathbf{v}$  the plasma flow and  $p$  the plasma pressure.

## 1.3 Magneto-hydrodynamic waves

There are many different forms of waves to be found in a plasma, both electromagnetic, sound and combinations of the two of them. Waves also differ in type and properties depending on the plasma parameters. The wave modes presented herein are for cold plasmas (where the plasma pressure is negligible in comparison to the magnetic pressure,  $B^2/2\mu_0$ ) as they are the simplest ones to deal with analytically, but similar types of waves are found in all plasmas.

By considering slight perturbations in a stationary plasma, the following dispersion relations for linear waves can be deduced ([1]):

$$[(w/k)^2 - v_A^2 \sin^2 \theta]u_x + [v_A^2 \sin \theta \cos \theta]u_z = 0 \quad (1.10)$$

$$[(w/k)^2 - v_A^2 \cos^2 \theta]u_y = 0 \quad (1.11)$$

$$[(w/k)^2 - v_A^2 \cos^2 \theta]u_z + [v_A^2 \sin \theta \cos \theta]u_x = 0 \quad (1.12)$$

$$v_A = \sqrt{\frac{B^2}{\mu_0 \rho}} \quad (1.13)$$

where  $\mathbf{k} = k\mathbf{e}_x$  represents the propagation vector of the wave,  $\mathbf{u}$  the plasma displacement and  $v_A$  the Alfvén velocity. The magnetic field has been defined as  $\mathbf{B} = (B \cos \theta, 0, B \sin \theta)$ . There are two different solutions to the dispersion relation to be found:

$$\begin{cases} (w/k)^2 &= v_A^2 \cos^2 \theta \\ u_x &= 0 \\ u_z &= 0 \end{cases} \quad (1.14)$$

$$\begin{cases} (w/k)^2 &= v_A^2 \\ u_y &= 0 \end{cases} \quad (1.15)$$

The first one is labelled the Shear-Alfvén wave mode and sets the plasma in a motion perpendicular to the propagation vector and the background magnetic field. The second one is referred to as a compressional or magnetoacoustic wave (in warm plasmas both a fast and a slow mode of the compressional waves exist), as it compresses the plasma in the direction of  $\mathbf{k}$ .

## 1.4 Frozen-in field lines.

A special characteristic for plasmas with a conductivity, characteristic length ( $l_c$ , the extent of the plasma) and particle velocity satisfying the magnetic Reynolds-number condition (1.16), are that the field lines can be considered as frozen in into the plasma, see [2] for more details.

$$R_m = \mu_0 \sigma l_c v_c \gg 1 \quad (1.16)$$

This means that a magnetic field line connecting a flux tube of plasma in space, will always connect the same population of plasma, no matter how it moves. The field lines will thus be deformed by the plasma flow.

## 1.5 Collisionless shocks

If a high velocity plasma population flows into a region of low velocity or static plasma, the magnetic field will serve to bind the particles together much like an ordinary gas causing them to collide and form a shock that separates the different regions, even if the plasmas themselves are so rarefied that no collisions should take place. Such collisionless shocks are for example to be found in front of all magnetised bodies located in the solar wind flow, such as the Earth, or in between two flows in the solar wind with different velocities (see section 5.1 for a more extensive analysis). One defines the region of plasma flowing into the shock as the upstream side, and the region flowing out of it as the downstream side. As the solar wind exceeds both the Alfvénic speed and the speed of sound, this shock front will cause nonlinear waves flowing with a speed greater than

the basic wave speeds (sonic-, compressional- or shear-Alfvénic waves) on the upstream side, and subsonic/subalfvénic waves on the downstream side of the shock ([1]).

## Chapter 2

# Cosmic Plasmas

Plasma is the dominant state of matter in space, where it exists in many different shapes and forms. In general, the cosmic plasmas are very tenuous, even more rarefied than what we normally refer to as vacuum. This low density leads to a more or less collisionless environment, allowing the plasma velocity distribution to take an arbitrary form, not necessarily the Maxwell distribution of normal gases. On the other hand, as the plasma consists of charged particles, the Coulomb and magnetic forces allows for particle interaction on larger scales instead.

### 2.1 The solar wind

The high temperature (about  $10^6$  Kelvin) of the solar corona causes solar particles such as protons, electrons and  $\text{He}^{2+}$  ions to accelerate into interplanetary space, creating a radial flow called the solar wind. Due to a high magnetic Reynolds number the magnetic field lines will be frozen-in into the flow and as the sun rotates, the interplanetary magnetic field will be stretched by the rotation and take the form of an Archimedes spiral, though with significant temporal and spatial variations. Some basic parameters of the solar wind can be found in the table below:

Solar Wind Parameter	Typical value
bulk speed	450 km/s
proton density	$6.6 \text{ cm}^{-3}$
sound speed	60 km/s
Alfvén speed	40 km/s

Table 2.1: Typical solar wind values near the orbit of Earth (1AU) ([1])

### 2.2 The Ionosphere

Seen from Earth, the cosmic plasma starts at the ionosphere, a layer of the atmosphere ranging from about 90 to 1500 km above the surface of the Earth.

This plasma exists mostly due to ultraviolet radiation emitted from the Sun, causing particles in the upper atmosphere such as oxygen and nitrogen to ionise and thus form a rather high density plasma. As the ionisation is caused by solar radiation, particles are ionised during daytime and recombine at night. This causes the density and extent of the ionosphere to differ both diurnally and around the globe.

## 2.3 The Magnetosphere

Succeeding the ionosphere is the magnetosphere, the area in space where the Earth's magnetic field is dominant over the interplanetary field. The field is in origin a dipole field centred at the Earth's core with the axis tilted about 11 degrees in respect to the rotational axis (a displacement that slowly changes with time). The interaction with the solar wind does however alter the shape of the magnetic field quite drastically: The magnetosphere is considerably compressed on the day-side of the globe by the solar wind (see chapter 4.1 for more details), but in return stretched out into a long tail on the night-side. As the density and temperature of the plasma varies greatly within these areas, the magnetosphere can be divided into several different sub-parts, as seen in figure 2.1.

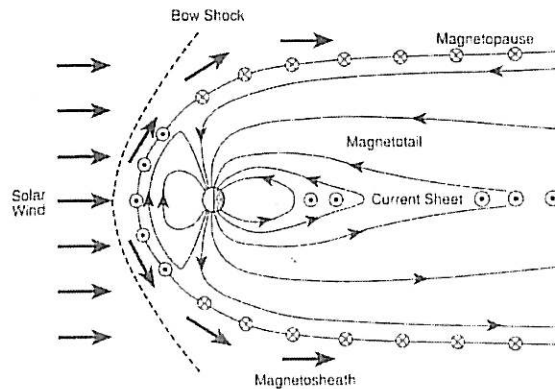


Figure 2.1: The Magnetosphere

### 2.3.1 Van Allen radiation belts

In a magnetic dipole field, there exists ring formed particle trajectories which (in theory) neither can be entered nor left. In the magnetosphere, these areas are known as the Van Allen radiation belts. The belt closest to Earth consists of positive ions (mainly  $H^+$  and  $O^+$ ), which forms a ring shaped current flowing westward around the magnetic equatorial plane. The ions inside are trapped in the belt for a long period of time, their entry and exit could for example be caused by particle collisions or disruptions in the magnetic field.

## Chapter 3

# Data acquisition

### 3.1 The ACE and Wind satellites

The Advanced Composition Explorer (ACE) satellite is designed to study the plasma in the solar wind. It is fairly stationary, orbiting around the L1 libration point where gravitational pull of the Earth and the Sun are in balance for an object with an orbit around the Sun of one Earth-year. This point is situated about 1.5 million kilometres away from Earth, on the Sun-Earth axis. ACE measures a wide variety of parameters, of which primarily the bulk speed and the plasma proton density has been of use in this thesis.

WIND is another satellite used for measuring solar wind properties. It was situated at the L1 libration point at first but now with the existence of ACE its orbit has been changed to a quite complex pattern around Earth. It is at some stages inside the magnetosphere, during which time-periods it is unsuitable for solar wind measurements.

### 3.2 SANA E pulsation magnetometer

As a part of the South African national Antarctic program, there is a pulsation magnetometer at the SANA E IV (South African National Antarctic Expedition) base. It consists of two induction coils, converting geomagnetic pulsations into voltage. The coils are separated by a 90 degree angle, each aligned along a magnetic axis. The equipment samples at a rate of 1 Hz, and has been designed to measure pulsations with periods ranging from 0.3 seconds to 5 minutes. As the magnetometer measures pulsations in voltage, calibration values for mV-nT transformations are presented in table 3.1.

Freq mHz	chan1 mV/nT	chan 2 mV/nT
10	43.4	44.7
20	61.9	63.6
50	64.3	66.3
100	68.3	70.2
200	64.4	66.4
500	43.6	42.1

Table 3.1: Calibration data for the SANA E pulsation magnetometer. Channel 1 is the north-south coil and channel 2 the east-west coil.

### 3.3 Absolute magnetometers

There are several stations around the earth that measures the absolute level of the surface magnetic field. An important characteristic of a magnetometer-station is the L-value. It signifies the length of the field-line incident at that particular point, and is measured as the distance in earth radii from the Earth's centre to the point where the field line crosses the magnetic equator.

The L value can be calculated using the following formula:

$$L = \cos^{-2} \lambda \quad (3.1)$$

where  $\lambda$  is the geomagnetic latitude where the field line surfaces.

Station	Geographic position		Geomag. latitude	L value
Hermanus	19.13 E	34.25 S	42.35 S	1.8
Kakioka	140.18 E	36.23 N	26.0 N	1.2
SANA E	2.83 W	71.67 S	61.35 S	4.35

Table 3.2: The magnetic and geographic properties of the magnetometer stations used in the thesis ([4],[5])

#### 3.3.1 The Dst-index

The Dst-index exists to give an image of global fluctuations in the magnetic field. It is based on the measurements of four different absolute magnetometers: Hermanus, San Juan, Kakioka and Honolulu, all of them located sufficiently distant from both the auroral and equatorial electrojets (ring currents) and with an appropriate distribution in longitude as well. The Dst-index value is an hourly average of the four, normalised to the dipole equator. It represents a disturbance field along the magnetic dipole axis, located at the Earth's surface, and is for example used to determine the occurrence of magnetic storms ([4]).

## Chapter 4

# Magnetosphere and solar wind interaction

### 4.1 The magnetopause

The dynamic pressure (which in the solar wind is approximately equal to the momentum flux) of the solar wind compresses the magnetosphere, causing it to shrink in size but increase in strength. This will in turn create a larger internal magnetic pressure inside the magnetosphere, which exerts an outward force on the field lines as well. The size of the magnetosphere can thus be described as an equilibrium state where the two pressures are equal in size ([1]):

$$\rho_{sw} v_{sw}^2 = B_m^2 / 2\mu_0 \quad (4.1)$$

where  $\rho_{sw}$  and  $v_{sw}$  are solar wind density and velocity and  $B_m$  the magnetospheric magnetic field. It is then obvious that the shape and size of the magnetosphere changes with the density and velocity of the solar wind. Normal values of the dayside border of the magnetosphere (often called the standoff distance) are about 8-12 Earth radii.

#### 4.1.1 The magnetopause current

There is a thin border at the edge of the magnetosphere called the magnetopause. It serves as an effective obstacle for the solar wind, deflecting most of the charged particles, forcing them into an interplanetary current around the Earth instead. This can be explained the following way:

As the Earth's magnetic field suddenly becomes dominant over the interplanetary field, a particle with the speed  $v$  will be affected by a Lorentz-force:

$$\mathbf{F} = q(\mathbf{v} \times \mathbf{B}) \quad (4.2)$$

This force will cause the electrons and ions to turn and move in opposite directions until they both eventually move anti-parallel to the solar wind inflow, see figure 4.1. The difference in the direction of rotation for the electrons and ions will create a current sheet around the magnetopause.

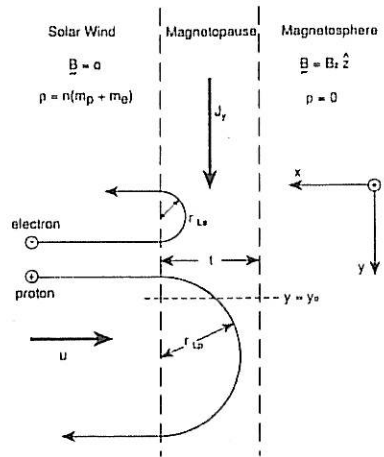


Figure 4.1: The Magnetopause current

## 4.2 Magnetic storms

The geomagnetic activity is closely linked to events in the solar wind, but their interplay is of a quite complex nature and depends on many factors such as the direction and strength of the interplanetary magnetic field. Also, a large and instant increase in the solar wind momentum flux can cause a sequence of large geomagnetic fluctuations, a magnetic storm. The following effects should to some degree be found for such an event:

- As the momentum flux increase strikes the magnetosphere, the border of the magnetosphere will be compressed and move closer to Earth
- As the number of charged particles in the solar wind increases, so will the magnetopause current.
- The new location and strength of the magnetopause current will give a positive contribution to the ground magnetic field, and the time of its occurrence is referred to as a sudden storm commencement.
- Some particles will be injected into the Van Allen radiation belts, energising the ring current. This will in turn lead to a significant decrease of the ground magnetic field, as the ring current flows in the opposite direction of the magnetopause current, and will thus yield a magnetic field that counteracts the ground magnetic field. This is known as the storm main phase, and normally takes place some hours after the initial stage.
- Particles will then gradually escape from the Van Allen belts, until a level of equilibrium has been restored.

## Chapter 5

# Methods of Analysis

The aim of this thesis has primarily been to investigate how perturbations in the solar wind momentum flux affects the pulsation magnetometer at the SANA station, if there are any pulsations to be seen, their frequency and duration. This has been done in the following manner:

1. Density and bulk speed data from the ACE satellite have been analysed in order to locate sudden increases in the solar wind momentum flux ( $\rho u^2$ ).
2. As the data from ACE is solely a point measurement in space, it is incapable of determining the spatial extent of the observed perturbation. To make sure that events observed with ACE will have an impact on Earth, the DST-index and local absolute magnetometers are monitored in the time following the event, in search for coherences.
3. It is then confirmed whether the time of the geomagnetic event is in conformity with the estimated impact time of the solar wind perturbation.
4. If all steps above turn out positive, the pulsation magnetometer at SANA is observed for the corresponding time period.

### 5.1 Shock speed

In this thesis, shocks found within the solar wind have been modelled in the following way:

As described in section 2, the velocity distribution in the solar wind is not confined to a Maxwell distribution and can have an arbitrary form. Based on this, the shock front has been regarded as a plasma population of constant density  $\rho_s$  and speed  $v_s$  moving through a background plasma of density  $\rho_0$  and speed  $v_0$ , where  $v_0 < v_s$ .

As the measurement of the bulk speed made by ACE uses an integration of the velocity distribution, the value of the plasma speed at the time of the shock found in the ACE data,  $v_{ACE}$  would then be a linear combination of  $v_s$  and  $v_0$ . An approximated shock speed can thus be calculated using the following formula:

$$\rho_{ACE} = \rho_s + \rho_0 \quad (5.1)$$

$$v_{ACE} = \frac{v_s \rho_s + v_0 \rho_0}{\rho_{ACE}} \quad (5.2)$$

$$v_s = \frac{v_{ACE} \rho_{ACE} - v_0 \rho_0}{\rho_s} \quad (5.3)$$

This is a very simplified way of modelling a shockfront though, as the densities and speeds often are far from constant at the time before and after the shockfront has passed. It is also unclear how the density and speed changes on a spatial scale, but the method seems to be accurate enough for the purpose.

### 5.1.1 Method of mass flux conservation

The result obtained above can also be verified by considering the mass flux passing through a shock ([3]). As the mass flux is to be equal on both sides of the shock, the following relation must be satisfied:

$$\rho_u (\mathbf{V}_u - V_s \hat{\mathbf{n}}) \hat{\mathbf{n}} = \rho_d (\mathbf{V}_d - V_s \hat{\mathbf{n}}) \hat{\mathbf{n}} \quad (5.4)$$

Where left hand side is the plasma flowing into the shock, and the right hand side the plasma flowing out of it.  $\mathbf{V}_u, \rho_u$  and  $\mathbf{V}_d, \rho_d$  represents the upstream and downstream propagation speeds and densities of the shock and  $\hat{\mathbf{n}}$  denotes the shock normal, which can be approximated as:

$$\hat{\mathbf{n}} = \frac{\mathbf{V}_d - \mathbf{V}_u}{|\mathbf{V}_d - \mathbf{V}_u|} \quad (5.5)$$

Then, the shock speed  $V_s$  can be expressed with the help of equation 5.4:

$$V_s = \frac{\Delta(\rho \mathbf{V})}{\Delta \rho} \cdot \hat{\mathbf{n}} \quad (5.6)$$

Which is compatible with the result obtained in 5.3, with the slight difference that it also considers the shock normal, i.e., direction in which the shock propagates. With the solar wind flow being primarily along the  $\mathbf{e}_x$  axis (defined as the basis vector of the Sun-Earth line) for both  $\mathbf{V}_u$  and  $\mathbf{V}_d$ ,  $\hat{\mathbf{n}}$  can be considered to be equal to  $\mathbf{e}_x$ .

### 5.1.2 WIND Measurements

A third way of determining the speed of a shockfront is to measure it at two different points in space and to compare their difference in time and distance. This type of calculation has been done with the help of the WIND satellite at the events when it has been located at a favourable position in space. The calculation of the propagation speed of the shock front is straightforward:

$$\Delta x = x_{ACE} - x_{WIND} \quad (5.7)$$

$$\Delta t = t_{ACE} - t_{WIND} \quad (5.8)$$

$$v_s = \Delta x / \Delta t \quad (5.9)$$

where  $x_{ACE}$  and  $x_{WIND}$  represents the satellites x-coordinates, and  $t_{ACE}$ ,  $t_{WIND}$  the time of the observed event.

## Chapter 6

# Analysing the data

### 6.1 Studied time period and data sources:

A time period of one year was chosen to for analysis, starting February 19, 2003 and ending February 18, 2004. The reason for this specific choice was the continuous data available from the SANA E pulsation magnetometer, only minor interruptions in the data flow are found during this period of time.

In addition to data collected by the pulsation magnetometer, provided by the university of KwaZulu-Natal, the following sources have been used:

- ACE proton density and solar wind bulk speed, provided by NASA  
<http://cdaweb.gsfc.nasa.gov/data>
- WIND proton density, provided by NASA  
<http://cdaweb.gsfc.nasa.gov/data>
- DST index data, provided by WDC-C2 Kyoto  
<http://swdcd.b.kugi.kyoto-u.ac.jp/dstdir/>
- Absolute magnetometer data from the Hermanus and Kakioka stations, provided by NiCT  
<http://kogma.nict.go.jp/cgi-bin/geomag-interface>

#### 6.1.1 Corrupt data samples

Unfortunately, the data provided by the ACE satellite does contain corrupt samples at times, indicated by the value of  $-10^{31}$ . During the analysis these corrupt samples have been replaced by an interpolation of the neighbouring samples. Longer periods of corrupt data have been ignored completely.

### 6.2 Solar wind events

During the time period mentioned above, the proton density and solar wind bulk speed was thoroughly analysed in search for sudden and significant increases of the solar wind momentum flux, where both large changes in the absolute value

and percentage have been noted. To assure that the observed increase has an impact on the magnetosphere, that it isn't just a very local perturbation in the solar wind, the Dst-index has been monitored for the times of the events in search for indications of magnetic storms. The magnetospheric response expected is for the ground magnetic field to increase slightly the hour after the event was observed by ACE and then for it to decrease suddenly about ten hours later, though large variations from this pattern can exist.

Twelve events were found using this technique, listed in table 6.1. The time value given is for the occurrence at the ACE position in the solar wind, which varies slightly. Information of the ACE x-coordinate for each event can be found in table 6.2. The density and bulk speed values presented are approximated values for the time just before and after each event. For plots of the solar wind events along with the corresponding magnetometer response, see figures 6.1 to 6.11.

Date yyyy.mm.dd	$t_{ACE}$ UT	$v_0$ kms <sup>-1</sup>	$\rho_0$ cm <sup>-3</sup>	$v_1$ kms <sup>-1</sup>	$\rho_1$ cm <sup>-3</sup>
2003.03.20	4.33	680	1.7	775	2.75
2003.04.08	0.25	360	25	395	60
2003.08.17	13.7	430	10	505	15
2003.10.24	14.8	435	9	585	31
2003.10.24	20.6	600	25	600	40
2003.10.25	1.2	—	—	—	—
2003.10.31	10.4	1040	0.4	1040	1.5
2003.10.31	10.8	1010	2.7	1010	7.5
2003.11.04	6.0	500	4.5	720	20
2003.11.15	5.25	640	4	725	11
2003.11.20	7.45	440	7	600	23
2004.01.22	1.07	475	7.5	660	15

Table 6.1: Solar wind events.  $t_{ACE}$  is the time of the event in the ACE data,  $v_0$  and  $\rho_0$  represents approximated values of the solar wind speed and proton density slightly before the shockfront,  $v_1$  and  $\rho_1$  slightly after it

Some of these events classifies without doubt as collisionless shocks, other are merely increases in speed and/or density. However, the classification is not of great importance, as they all cause a magnetospheric reaction. Neither velocity nor density data have been included for the event of 2003.10.25, as it is a very slow increase which makes the start and stop values of little interest.

### 6.3 Magnetometer data

To get a better picture of the magnetospheric reaction to the solar wind event, data from individual absolute magnetometers have been studied as well. For all the events, a clear jump in the absolute magnetic field can be observed at both stations, but often of different amplitude. As there is no noticeable difference in impact time when comparing the stations to each other, an approximated time of impact can be measured for each event.

## 6.4 Propagation time calculations

The propagation time between ACE and the observed change of the absolute magnetometers has been calculated using the equation 5.3 and the solar wind values presented in table 6.1. The results are displayed in table 6.2. Even if the calculations are based on large approximations, the results obtained seem to be consistent with the observed lag times to a high degree, indicating that the events in the solar wind and magnetosphere are indeed related.

Date yyyy.mm.dd	$t_{ACE}$ UT	$v_{est}$ kms <sup>-1</sup>	$x_{ACE}$ Gm	$t_{est}$ UT	$t_{real}$ UT
2003.03.20	4.33	930	1.4	4.75	4.75
2003.04.08	0.25	420	1.43	1.2	1.15
2003.08.17	13.7	655	1.46	14.3	14.35
2003.10.24	14.8	645	1.47	15.45	15.35
2003.10.24	20.6	600	1.47	21.3	21.3
2003.10.31	10.4	1040	1.48	10.8	10.75
2003.10.31	10.8	1010	1.48	11.2	11.2
2003.11.04	6.0	785	1.49	6.5	6.4
2003.11.15	5.25	775	1.52	5.8	5.85
2003.11.20	7.45	670	1.53	8.1	8.15
2004.01.22	1.07	845	1.46	1.55	1.6

Table 6.2: Solar wind speed estimates using formula 5.3.  $t_{ACE}$  is the time of the event in the ACE data,  $v_{est}$  the estimated velocity,  $t_{est}$  an estimated impact time based on the ACE position and the estimated solar wind speed.  $t_{real}$  is the impact time observed by the absolute magnetometers.

## 6.5 Solar wind speed calculations using WIND

As mentioned in section 5.1.2, the solar wind propagation speed can be calculated by using WIND as well. This is however only feasible when the satellite is in a propitious position in space. At the periods of time when it is found inside the magnetosphere it cannot supply any solar wind data, which makes the analysis impossible. At other times when it is fairly close to ACE, perturbations alike those presented for the ACE data can be observed with WIND as well, but as the distance and time in between is fairly small, spatial fluctuations of the solar wind will give rise to large errors, making the approximation useless. The speed estimates in the table below have been calculated with formula 5.9, and the estimated magnetospheric impact time has then been based on those speed estimates and the ACE position for the given time. Most of the events give a fairly reasonable solar wind velocity with this method as well. Plots of the WIND proton density for each events that satisfies the conditions sought are displayed in figure 6.5.

No data were available for the event of 2003.08.17. For the events of 2003.03.20 and 2003.04.08, WIND was in the vicinity of ACE, making the propagation speed calculations impossible.

Date yyyy.mm.dd	$x_{WIND}$ Gm	$\Delta x$ Gm	$t_{WIND}$ UT	$\Delta t$ h	$v_{est}$ kms <sup>-1</sup>	$t_{est}$ UT	$t_{real}$ UT
2003.10.24	-0.86	2.33	16.8	2	323	16.05	15.35
2003.10.31	-1.05	2.53	11.45	0.65	1080	10.8	10.75
2003.11.04	-1.13	2.62	6.75	0.75	970	6.4	6.4
2003.11.15	-1.3	2.82	6.4	1.15	680	5.85	5.85
2003.11.20	-1.35	2.88	8.6	1.15	695	8.05	8.15
2004.01.22	-1.34	2.8	2.1	1.03	755	1.6	1.6

Table 6.3: Solar wind speed estimates using the WIND satellite and formula 5.9.  $x_{WIND}$  is the WIND x-position,  $t_{WIND}$  the time of the WIND measurement of the event,  $\Delta x$  and  $\Delta t$  are the distance and time difference between ACE and WIND.  $v_{est}$  is the estimated solar wind speed,  $t_{est}$  an estimated impact time based on the ACE position and the estimated solar wind speed.  $t_{real}$  is the impact time observed by the absolute magnetometers.

Figure 6.1: event of 2003.03.20

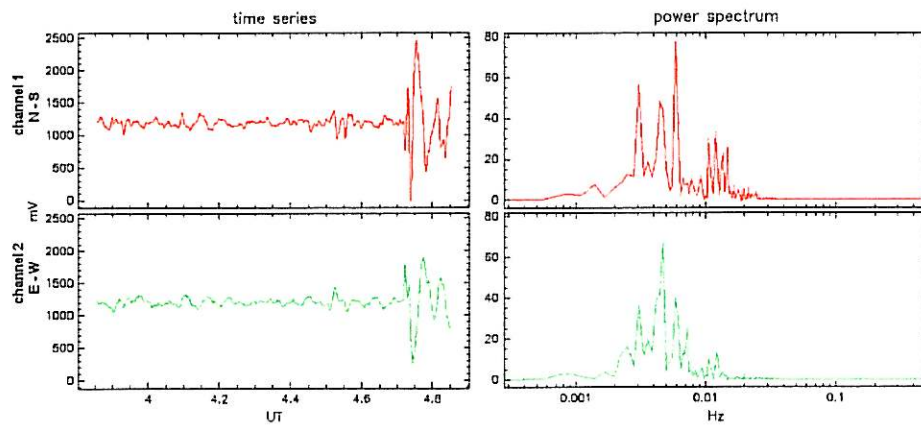
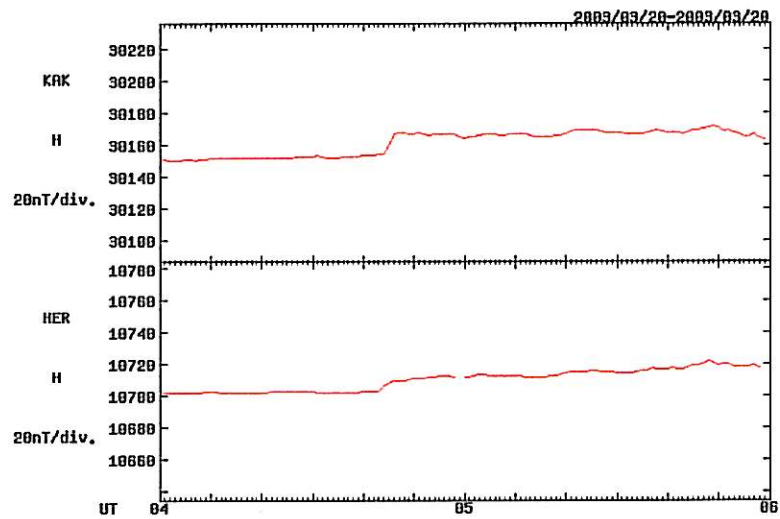
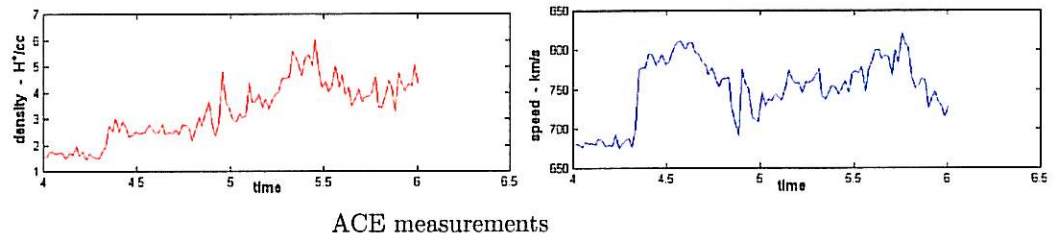
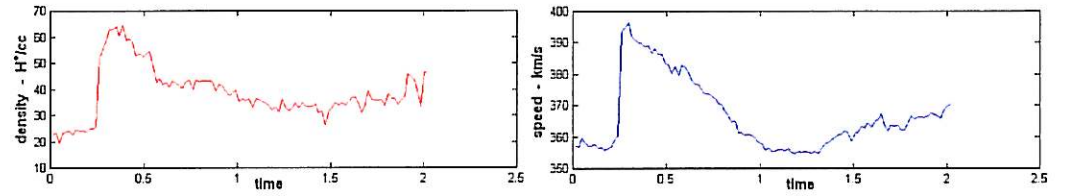
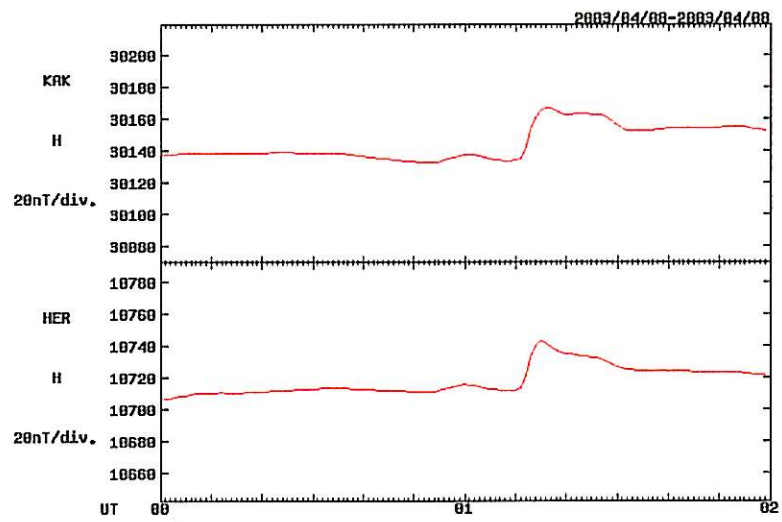


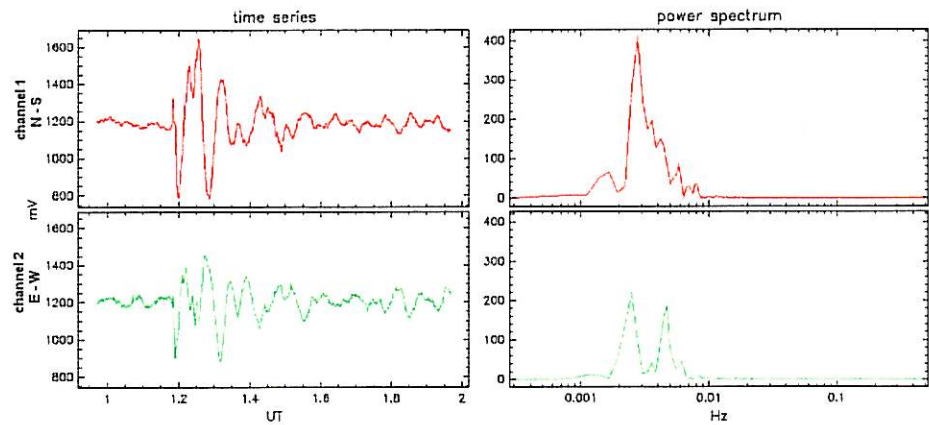
Figure 6.2: event of 2003.04.08



ACE measurements

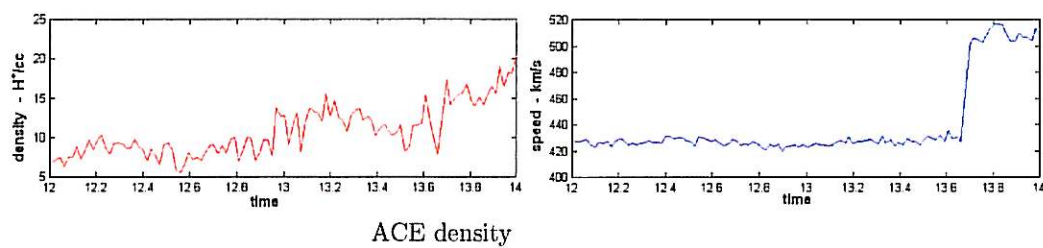


Absolute magnetometers at Kakioka and Hermanus

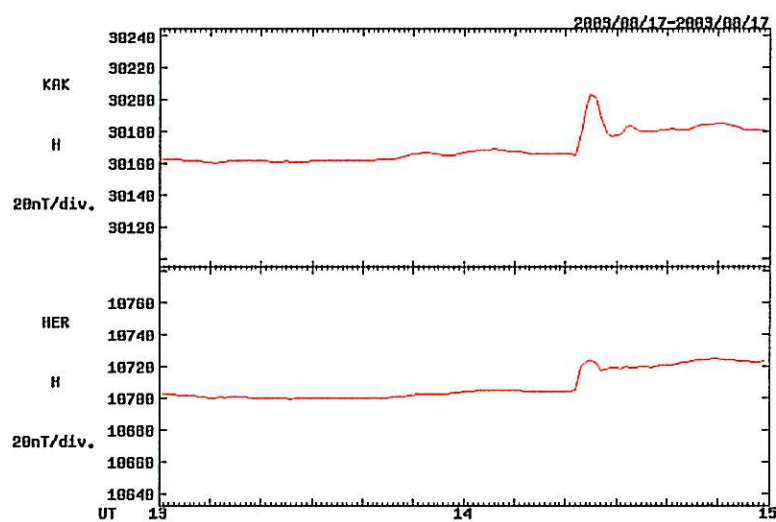


Pulsation magnetometer at SANAE

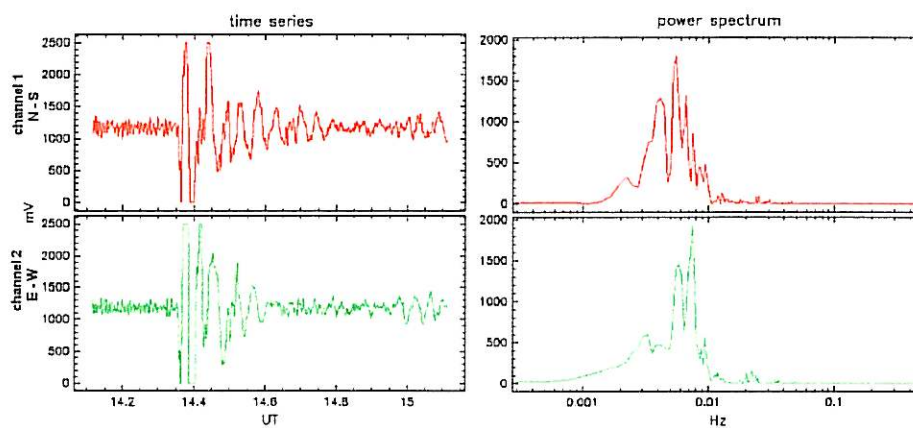
Figure 6.3: event of 2003.08.17



ACE density



Absolute magnetometers at Kakioka and Hermanus



Pulsation magnetometer at SANA

Figure 6.4: event of 2003.10.24

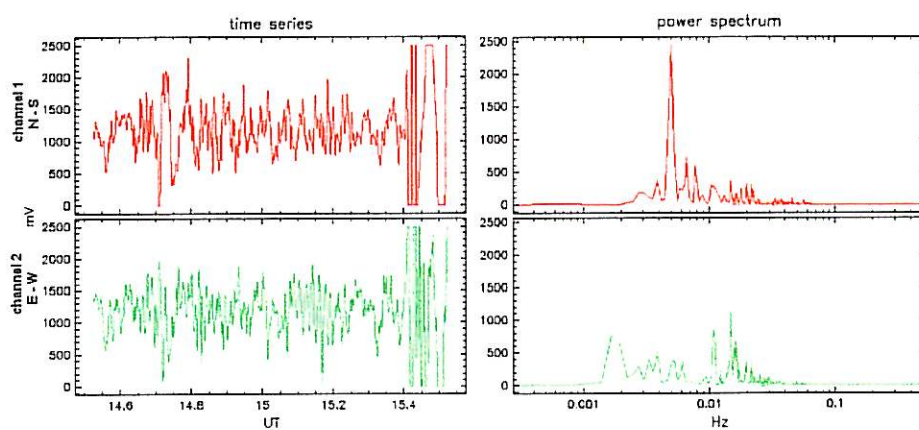
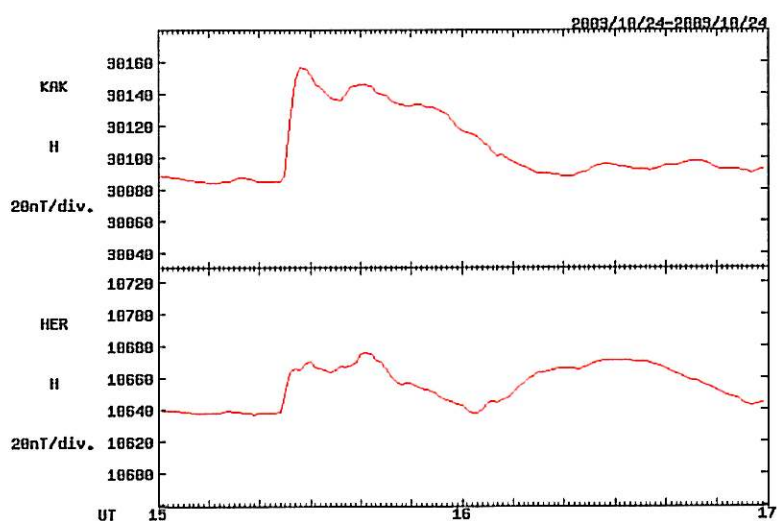
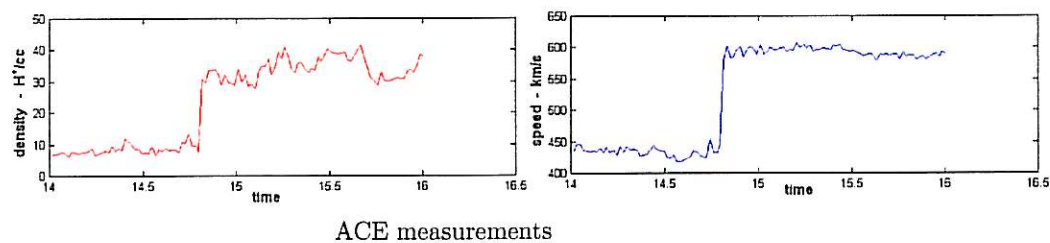
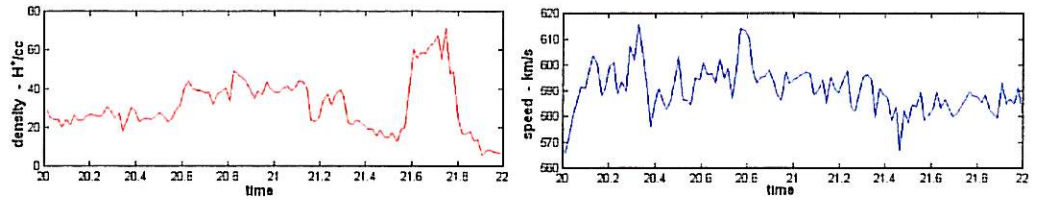
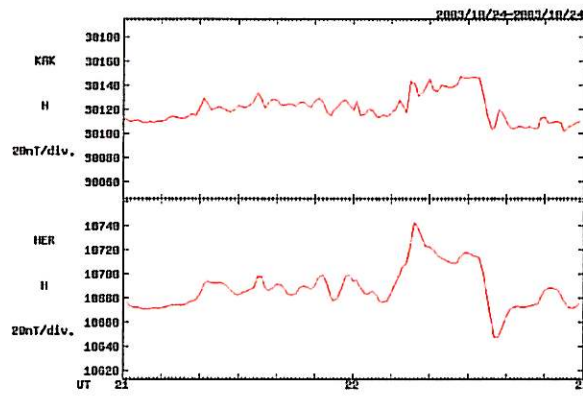


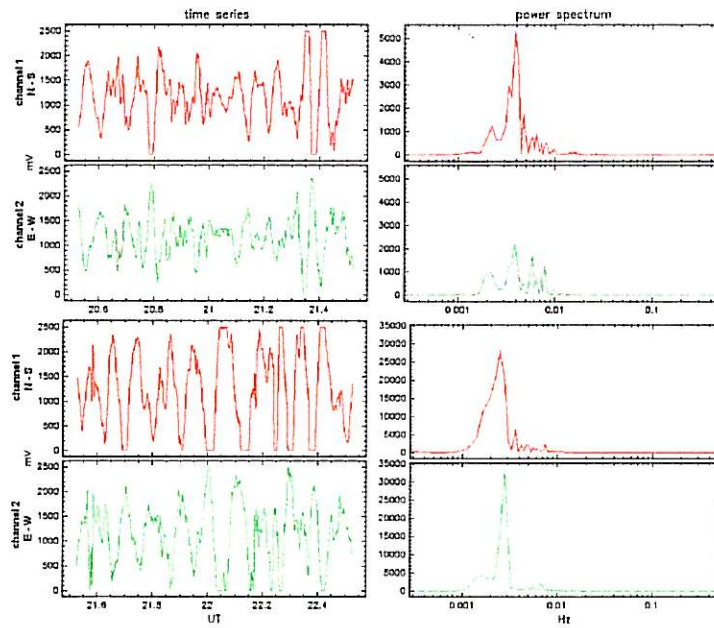
Figure 6.5: event of 2003.10.24



ACE measurements



Absolute magnetometers at Kakioka and Hermanus



Pulsation magnetometer at SANA

Figure 6.6: event of 2003.10.25

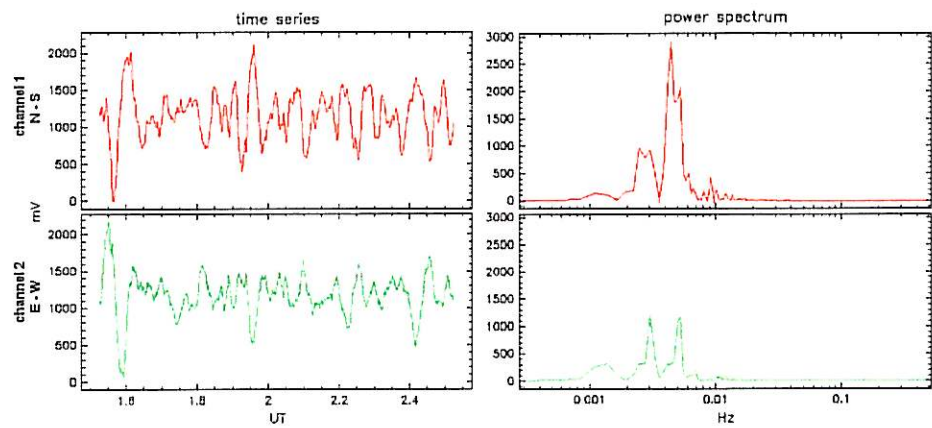
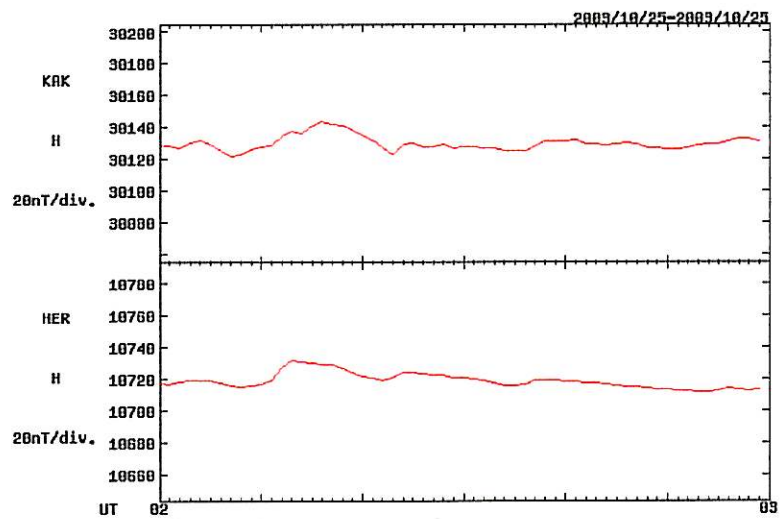
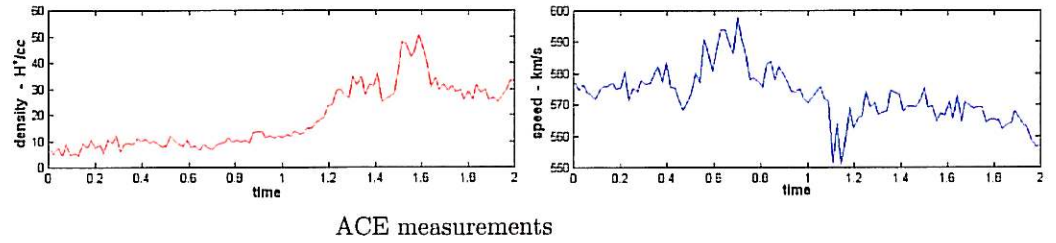
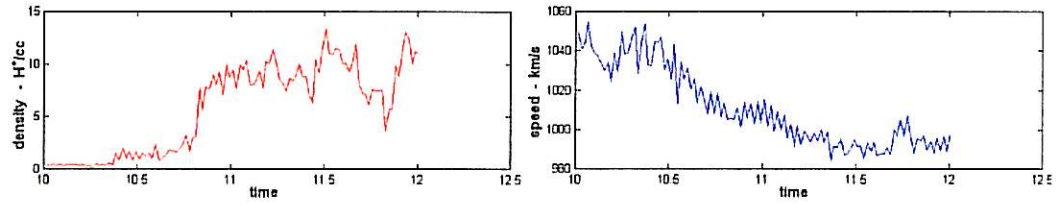
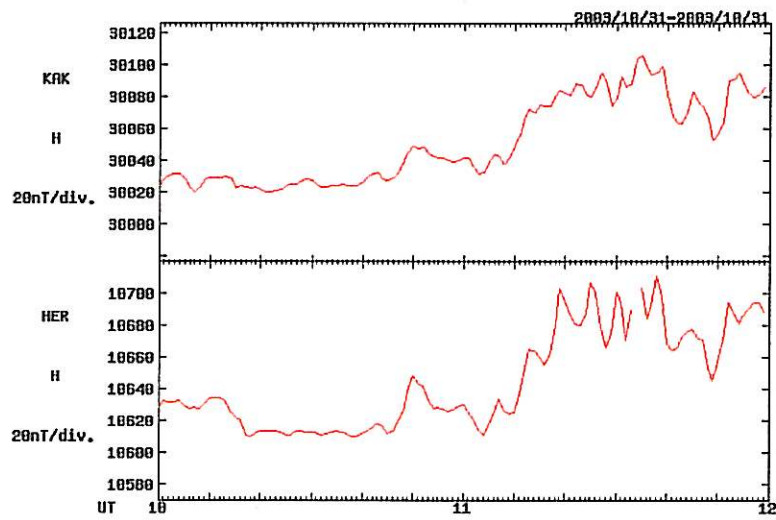


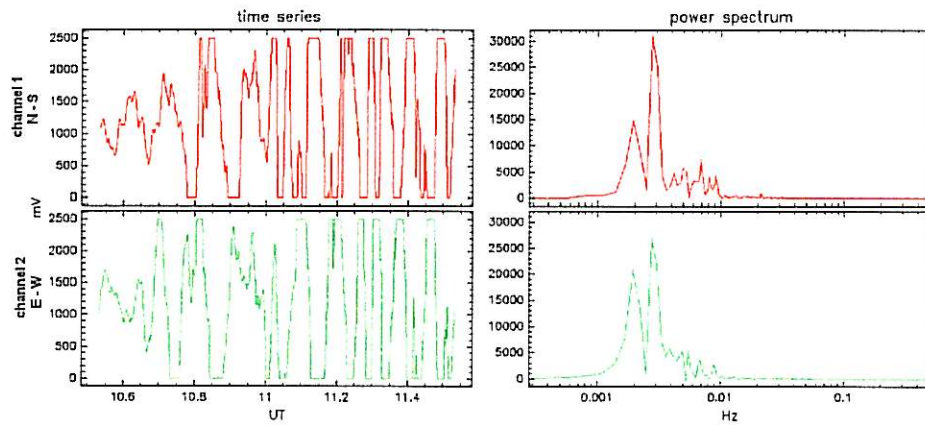
Figure 6.7: event of 2003.10.31



ACE measurements

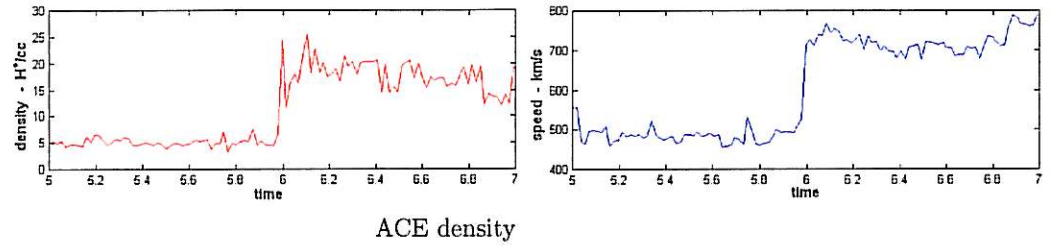


Absolute magnetometers at Kakioka and Hermanus

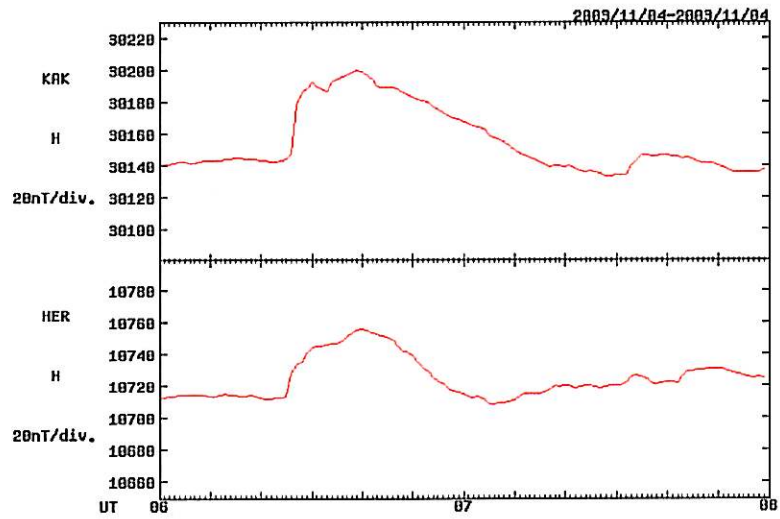


Pulsation magnetometer at SANA

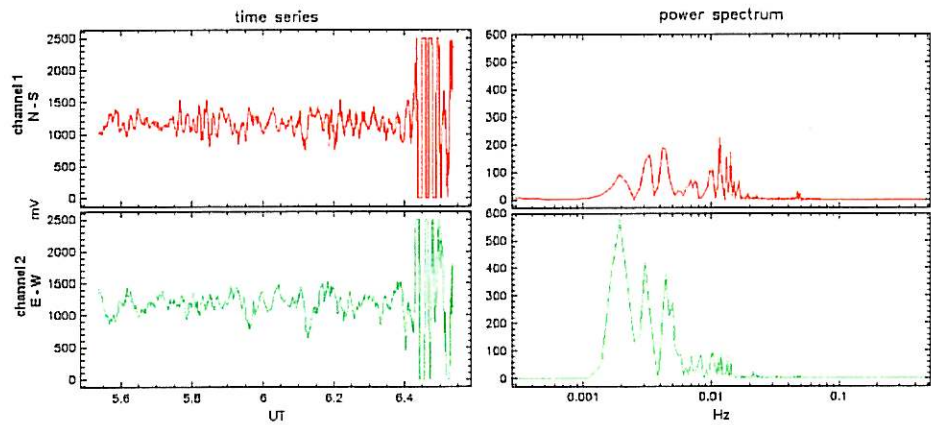
Figure 6.8: event of 2003.11.04



ACE density



Absolute magnetometers at Kakioka and Hermanus



Pulsation magnetometer at SANAE

Figure 6.9: event of 2003.11.15

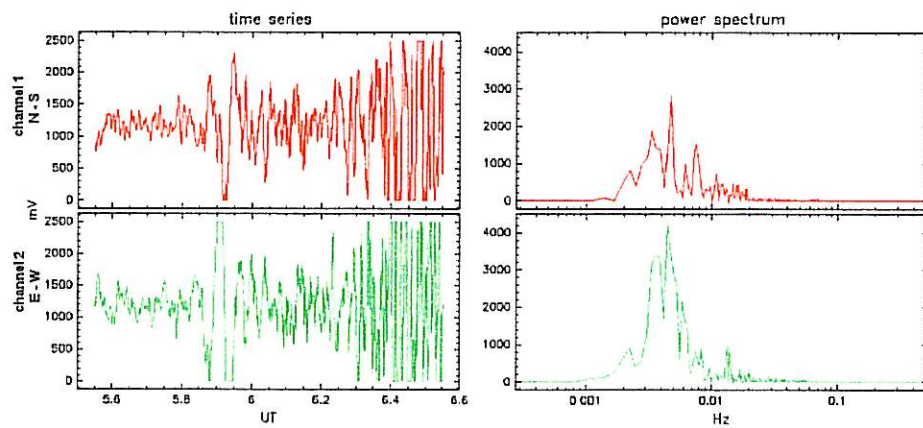
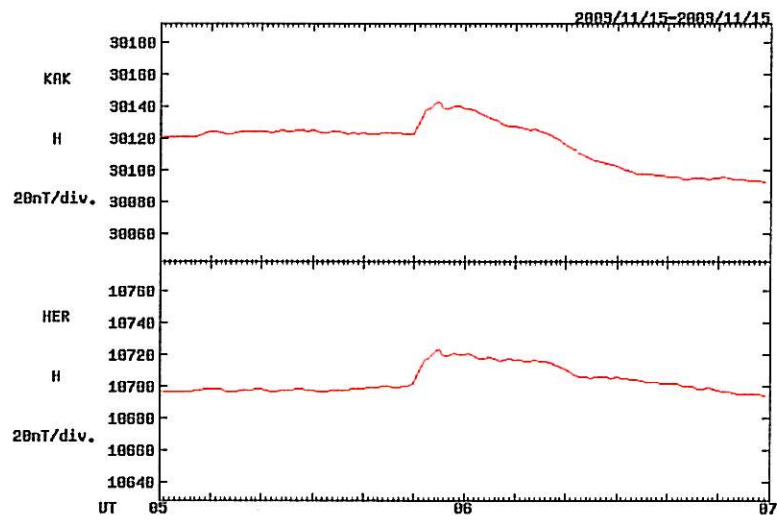
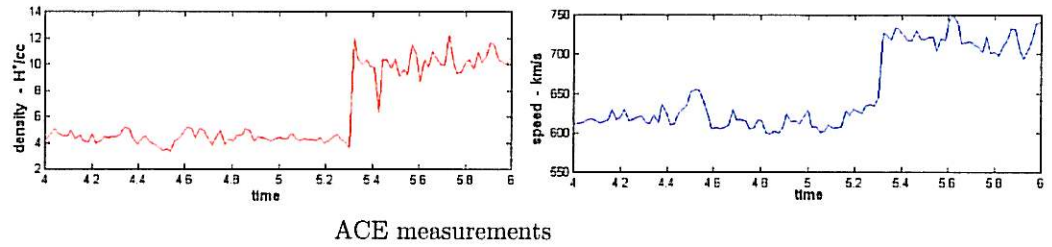
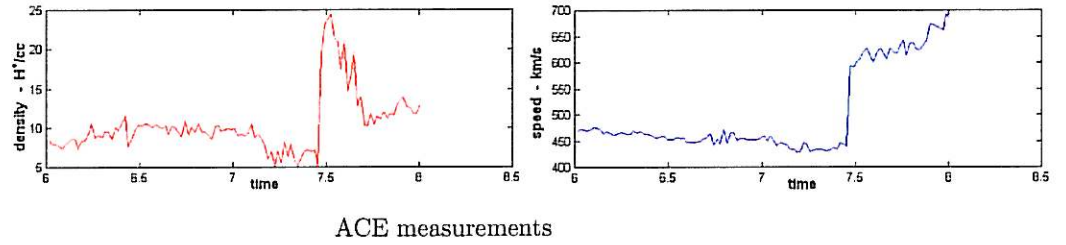
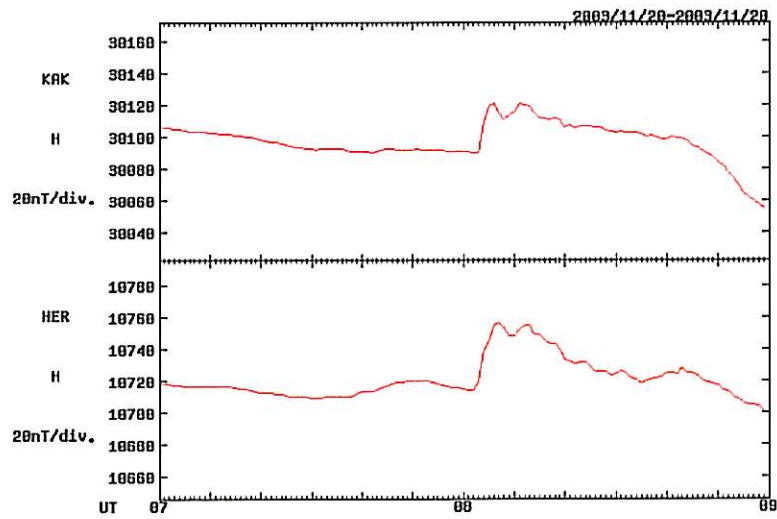


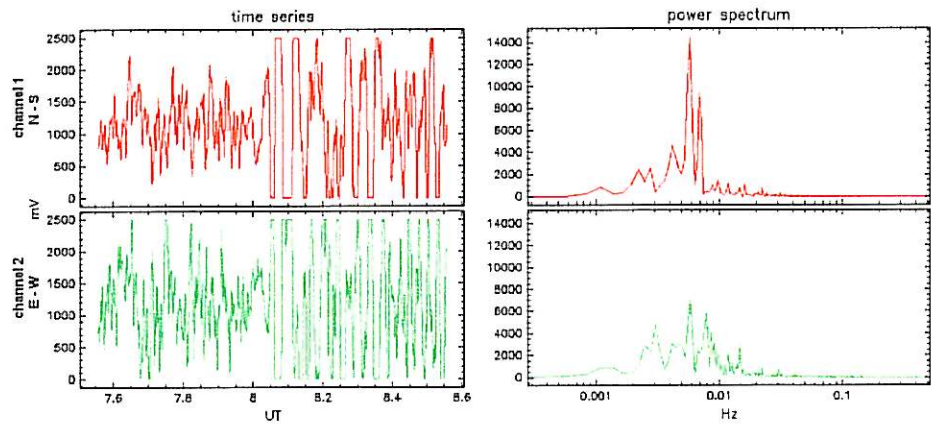
Figure 6.10: event of 2003.11.20



ACE measurements



Absolute magnetometers at Kakioka and Hermanus



Pulsation magnetometer at SANA

Figure 6.11: event of 2004.01.22

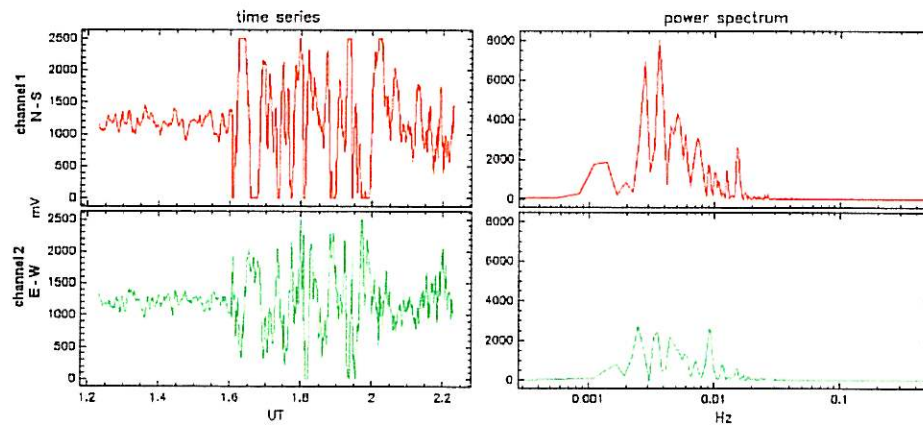
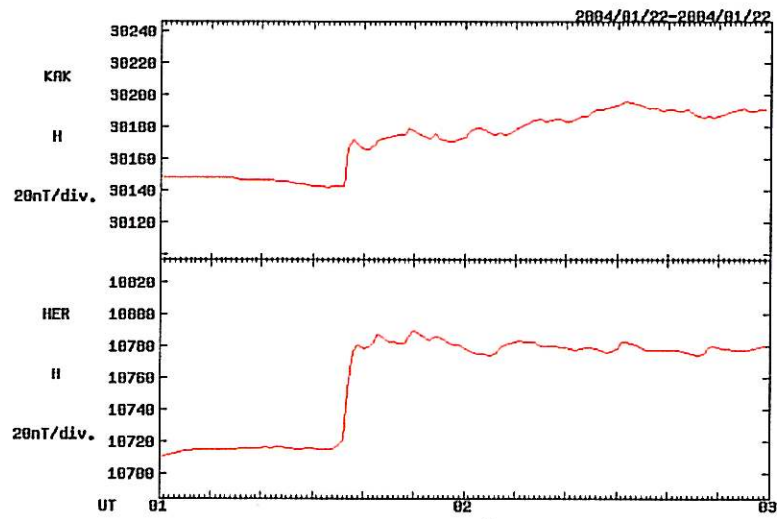
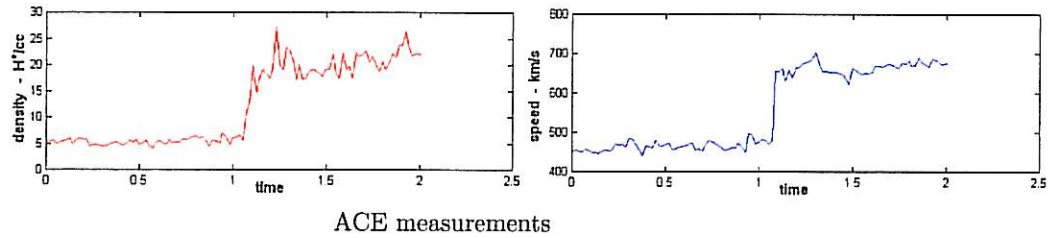


Figure 6.12: Dst index plots. The x-axes represent days of the month of the occurring event, the y-axes the Dst deviation in nT.

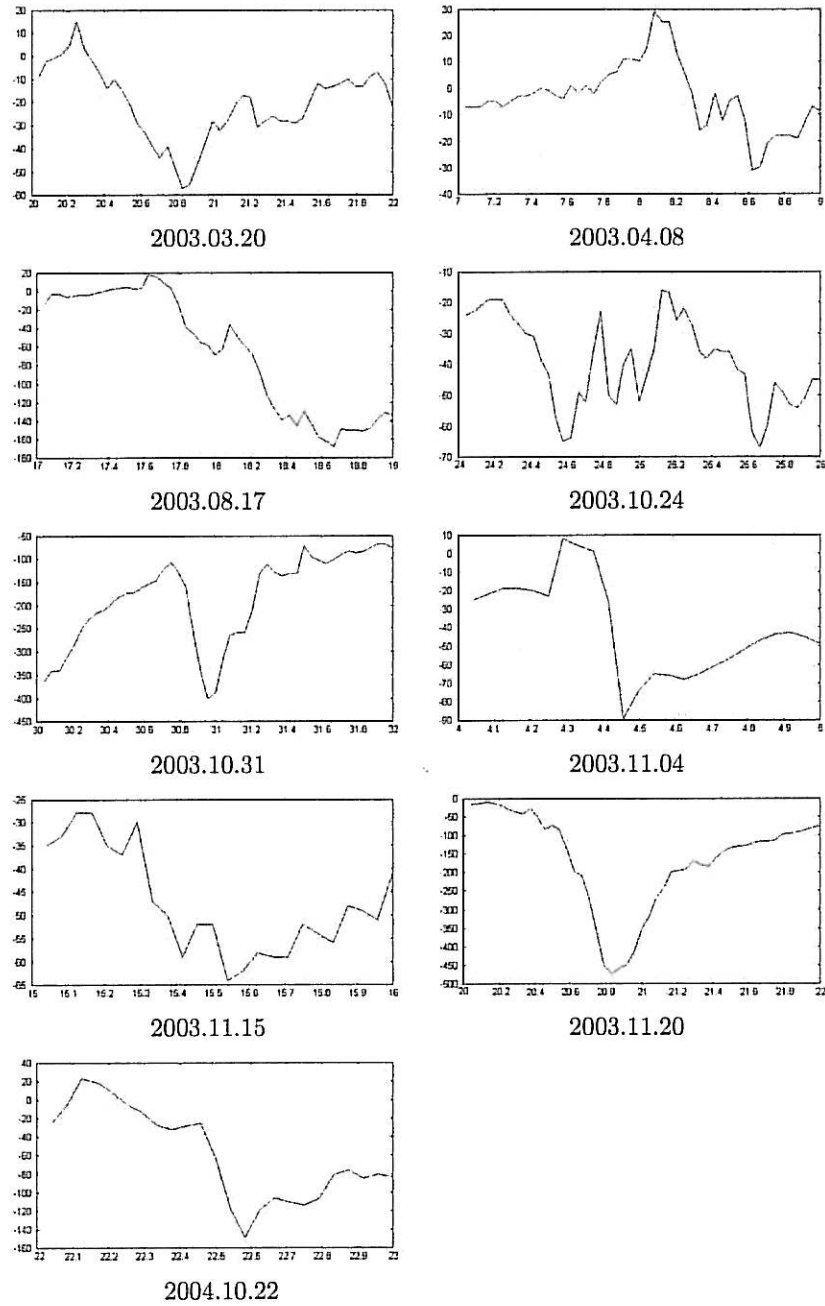
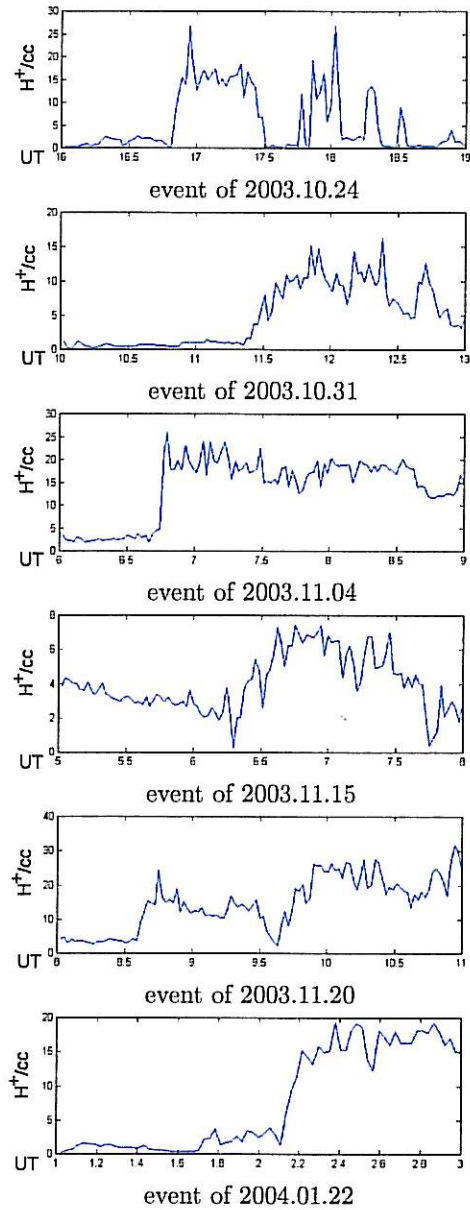


Figure 6.13: WIND proton density



## Chapter 7

### Comments

As most events show a clear relation between an increase in the absolute magnetic field and magnetospheric pulsations (or an increase of the amplitude of already existing pulsations), it is most probable that the momentum flux jumps in the solar wind works as a source for magnetospheric magneto-hydrodynamic waves, which is what we observe at SANA. The pulsations observed are of very varying amplitude, duration and frequency and no obvious connection between the absolute field increase, solar wind parameters and the character of the pulsations caused can be seen; additional events will be necessary to make a more thorough analysis. It is hard to draw any specific conclusions regarding the frequencies of the pulsations, as the magnetometer deviation often saturates moments after the initial response, something that will alter the shape of the signal and distort the frequency spectra. No clear peaks in frequency seems to exist though, which gives the pulsations a quite noisy character, but with main power in the PC5 spectra of 2-7 mHz.

#### 7.1 Magnetospheric propagation

In the calculations of the estimated impact time, no regard has been paid to the magnetospheric propagation time. Naturally, the wave propagation speed between the magnetopause to the magnetometers will be limited by the Alfvén velocity in the magnetosphere. Exactly how the waves are set up by the magnetospheric compression is unclear however, and will require thorough investigations.

#### 7.2 Event of 8 April

There is a large jump in solar wind momentum flux to be seen for this event, much comparable to the second event on October 24th in shape and size. The magnetospheric response however, is short and of limited amplitude. This indicates that there are many other factors of importance as well for how the magnetosphere responds to the impact of the solar wind events.

### 7.3 Events of 24-25 October

Several consecutive events are found during this time-period. The first one, occurring 2003.10.24 at 14.8 UT, is rather straightforward with increases in the solar wind momentum flux, absolute magnetic field value and pulsations. The second event, observed at 20.6 UT, two consecutive steps in the solar wind density are found (the latter one at 21.6 UT). They both seem to cause an absolute magnetic field increase. Unfortunately, the SANA E signal is already saturated at the time of the second step making observations of its consequences impossible.

The third one, occurring 2003.10.25, is a very slow but substantial increase of the plasma density. There is a reaction in the Dst index at the appropriate time, but as neither the Hermanus nor Kakioka station show any direct response to it the main effects must be around the San Juan and Honolulu longitudes. No pulsations can be observed at SANA E either.

### 7.4 Event of 31 October

According to the Dst-index, one of the largest magnetic storms of the year took place the day before the observed event of 2003.10.31. Unfortunately, the ACE data are corrupt for that period of time, making all observations impossible for that magnetic storm. The event studied consist of two consecutive steps in density. The first one is very small in magnitude, but large in relative terms. The second one much larger in magnitude. The absolute magnetometers show a pattern much like that of the solar wind proton density at the appropriate times. Whether they cause the pulsation increase seen in the SANA E data is hard to say, as the signal is saturated just before the first event and for a long time afterwards, making any observations of the consequences of the second jump impossible.

### 7.5 Event of 22 January

At this event, the Hermanus magnetic-field increases with the considerable amount of 80 nT, which is one the largest values among the observed events. The pulsation observed for the according time however are not as violent as many of the others, only the north-south component exceeds the maximum measurement value, and that at a few occasions only.

## 7.6 Conclusions

The character of the pulsations studied are of quite a wide variety and they differ in amplitude as well as duration, which can be affected by many other factors than just the solar wind parameters observed. It is important to remember that the change seen with ACE is representative for a specific point in space only, and it is not certain that neither the shape nor size for the part of the solar wind that is bound for Earth are similar to the event observed. This inconsistency can easily be confirmed by comparing the ACE data with WIND; even though the events are often quite alike, there are significant differences in amplitude as well as shape to be found.

Another factor that needs to be considered is the magnetic local time of the observed pulsation. The absolute field increase often seems to be greater in the dusk sector than elsewhere, making that area more likely to be affected by solar wind events.

One can also conclude that only a small fraction of the magnetospheric pulsations are connected with an increase of the absolute field value (and thus the solar wind momentum flux), as there are many more pulsations in the SANA data than there are events in the absolute magnetic field.

# Bibliography

- [1] Kivelson and Russel  
Introduction to space physics  
Cambridge University Press, 1995
- [2] Fälthammar  
Plasmafysik, 6th edition  
Alfvénlab, KTH, 2001
- [3] Paschmann and Daly  
Analysis methods for multispacecraft data  
International space science institute, 2000
- [4] Sugiura and Kamei  
on DST index  
IAGA Bulletin N°40, 1991
- [5] Magnetic Results 2002  
Hermanus magnetic observatory



ISSN 1103-6613  
TRITA-ALP-2005-01  
ISRN KTH/ALP-05/01-SE

ISSN 1103-6613  
TRITA-ALP-2005-01  
ISRN KTH/ALP-05/01-SE